Cytotherapy 25 (2023) 670–682

Contents lists available at ScienceDirect

CYTOTHERAPY

journal homepage: www.isct-cytotherapy.org

FULL-LENGTH ARTICLE
Manufacturing

Label-free *in vitro* assays predict the potency of anti-disialoganglioside chimeric antigen receptor T-cell products

Meghan Logun[1,2], Maxwell B. Colonna[4,5], Katherine P. Mueller[6], Divya Ventarapragada[1], Riley Rodier[1], Chaitanya Tondepu[1,2,3], Nicole J. Piscopo[6], Amritava Das[12], Stacie Chvatal[7], Heather B. Hayes[7], Christian M. Capitini[8,9], Daniel J. Brat[10], Theresa Kotanchek[11,#], Arthur S. Edison[4,5,#], Krishanu Saha[6,9,#], Lohitash Karumbaiah[1,2,3,*]

[1] *Regenerative Bioscience Center, University of Georgia, Athens, Georgia, USA*
[2] *Division of Neuroscience, Biomedical and Health Sciences Institute, University of Georgia, Athens, Georgia, USA*
[3] *Edgar L. Rhodes Center for Animal and Dairy Science, College of Agriculture and Environmental Science, University of Georgia, Athens, Georgia, USA*
[4] *Department of Biochemistry & Molecular Biology, Complex Carbohydrate Research Center, University of Georgia, Athens, Georgia, USA*
[5] *Institute of Bioinformatics, University of Georgia, Athens, Georgia, USA*
[6] *Department of Biomedical Engineering, University of Wisconsin-Madison, Madison, Wisconsin USA*
[7] *Axion BioSystems, Atlanta, Georgia USA*
[8] *Department of Pediatrics, University of Wisconsin School of Medicine and Public Health, Madison, Wisconsin USA*
[9] *University of Wisconsin Carbone Cancer Center, University of Wisconsin-Madison, Madison, Wisconsin USA*
[10] *Department of Pathology, Northwestern University Feinberg School of Medicine, Chicago, Illinois USA*
[11] *Evolved Analytics LLC, Rancho Santa Fe, California, USA*
[12] *Morgridge Institute for Research, Madison, Wisconsin, USA*

ARTICLE INFO

Article History:
Received 28 October 2022
Accepted 13 January 2023

Key Words:
CAR-T therapy
cellular Immunotherapy
glioblastoma
T-cell potency

ABSTRACT

Background aims: Chimeric antigen receptor (CAR) T cells have demonstrated remarkable efficacy against hematological malignancies; however, they have not experienced the same success against solid tumors such as glioblastoma (GBM). There is a growing need for high-throughput functional screening platforms to measure CAR T-cell potency against solid tumor cells.
Methods: We used real-time, label-free cellular impedance sensing to evaluate the potency of anti-disialoganglioside (GD2) targeting CAR T-cell products against GD2+ patient-derived GBM stem cells over a period of 2 days and 7 days *in vitro*. We compared CAR T products using two different modes of gene transfer: retroviral transduction and virus-free CRISPR-editing. Endpoint flow cytometry, cytokine analysis and metabolomics data were acquired and integrated to create a predictive model of CAR T-cell potency.
Results: Results indicated faster cytolysis by virus-free CRISPR-edited CAR T cells compared with retrovirally transduced CAR T cells, accompanied by increased inflammatory cytokine release, CD8+ CAR T-cell presence in co-culture conditions and CAR T-cell infiltration into three-dimensional GBM spheroids. Computational modeling identified increased tumor necrosis factor α concentrations with decreased glutamine, lactate and formate as being most predictive of short-term (2 days) and long-term (7 days) CAR T cell potency against GBM stem cells.
Conclusions: These studies establish impedance sensing as a high-throughput, label-free assay for preclinical potency testing of CAR T cells against solid tumors.

Introduction

Cellular immunotherapies have rapidly emerged as a new class of cancer treatments. Along with checkpoint blockade, the emergence of T cells that have been genetically modified to express chimeric antigen receptors (CAR) has brought new successes in cancer treatment. Since 2017, six CAR T-cell therapies have been approved by the Food and Drug Administration for treating B-cell acute lymphoblastic leukemia, large B-cell lymphoma, mantle cell lymphoma and multiple myeloma [1]. However, the successes in treating hematologic malignancies with CAR T-cell therapy have not been replicated in solid tumors for various reasons. As newer CAR T-cell products are

* Correspondence: Lohitash Karumbaiah, 425, River Rd., Athens, GA 30602.
E-mail address: lohitash@uga.edu (L. Karumbaiah).
Co-corresponding authors.

https://doi.org/10.1016/j.jcyt.2023.01.008

being designed against invasive solid tumors like glioblastoma (GBM), critical *in vitro* challenges prevent the identification of process parameters of CAR T-cell effectiveness, such as CAR T-cell proliferation, time to exhaustion, dosing strategy, and rate of target cell killing [2–8]. Although cellular product preparation, validation and supply chain transport are well-regulated, there are currently no uniform technical standards for CAR T-cell manufacturing or in-process potency testing. The lack of high-throughput, label-free methods to evaluate real-time CAR T-cell potency *in vitro* is a critical bottleneck that hinders the assessment of desirable quality attributes during manufacturing of cellular therapies.

Chromium 51 (^{51}Cr) release assays are considered the gold standard for monitoring immune cell–mediated killing and continue to be used to test CAR T-cell products today. Although ^{51}Cr release assays are sensitive, they represent an indirect measure of cell killing and need to be limited to short-term 4-h assessments to avoid risking spontaneous leakage of hazardous radioactive isotopes from the target cells [9]. Second, this method is not sensitive to measurements involving low effector-to-target (E:T) ratios and therefore requires very high E:T ratios to observe cell killing [9]. Other cytotoxicity assays commonly used include flow cytometry or fluorescent dye–based measurements of cell killing, and reporter assays or lactate dehydrogenase release, which involve genetically engineering the target cells with a fluorescent or bioluminescent reporter (which could affect realistic cell–cell interactions or behavior). Additional deficiencies include small target sample numbers or endpoint measurements that are not conducive to the parallel assay processing needed to gain insights into the multifaceted potency of effector cells.

Real-time, label-free cellular impedance sensing can be used to obtain dynamic measurements of cellular adhesion and subsequent cell-mediated cytotoxicity. Originally developed to monitor cell barrier formation and cellular motility, cellular impedance changes are now being used to sensitively measure cell proliferation, spreading, wound healing and cytotoxicity [10–16]. All cells exhibit passive electrical behaviors, owing to the presence of an insulating lipid bilayer separating ionic cytoplasm from ion-rich media that creates interfacial polarization under an applied field [17,18]. Therefore, when cells are cultured directly on electrodes embedded in the cell culture substrate, and a small alternating current is applied, the current flow is impeded between electrodes and the system impedance increases with cell coverage [19]. Adherent cell death and detachment therefore reduces the measured impedance, which is recorded by the impedance platform in real time [20–22]. While impedance is extremely sensitive to adherent cells, immune effector cells are nonadherent and do not directly affect impedance signal [23].

CAR T cells are traditionally manufactured using lenti- or retroviruses due to the high-efficiency of gene transfer. However, viral transduction can infer broad and nonspecific genomic integration that subsequently risks heterogeneous CAR expression, potentially leading to inadequate responses in the patient [24–27]. CRISPR/Cas9 genome editing can insert the CAR transgene into a specific genomic locus to reduce risks associated with insertional mutagenesis and ensure usage of a promoter that will yield high surface expression. Editing also can be multiplexed to rewire T-cell responses toward more potent T-cell phenotypes [28–31]. The combination of multiple *in vitro* assays encompassing both endpoint and temporal data can demonstrate differential cytotoxic potency of CAR T-cell products against patient-derived tumor cells.

Here we describe a non-invasive, label-free impedance assay to detect anti-cancer potency of retrovirally (RV) transduced and virus-free CRISPR-edited (VFC) CAR T-cell products [32] derived from matched donor T cells. RV and VFC CAR T cells targeting anti-disialoganglioside (GD2) were cocultured with patient-derived GBM stem cell (GSC) monolayers in multi-well impedance plates, and real-time, label-free changes in impedance as a measure of cytotoxicity were acquired continuously over 2 and 7 days *in vitro*. CAR T-cell–mediated GSC cytotoxicity was validated by measuring temporal differences in CAR T-cell activation and exhaustion immunophenotype, cytokine release and cellular infiltration into three-dimensional GBM spheroids. Results were further validated by conducting impedance biosensing of VFC and RV CAR T-cell potency against an additional GD2+ neuroblastoma line. Experimental results were subsequently evaluated using a symbolic regression predictive modeling software to identify indicators of CAR T-cell potency. These findings provide a template for real-time, label-free CAR T-cell potency assessment that can be adopted by the cell-manufacturing industry.

Methods

Cell Culture

GSCs (N08-30) were isolated from primary human GBM tissue, molecularly characterized and established in culture according to procedures approved by Emory University Institutional Review Board protocol 45796 (D.J.B). GSCs were maintained in Neurobasal A Medium (Thermo Fisher Scientific, Waltham, MA, USA) containing 1% penicillin–streptomycin and 0.5% L-glutamine and supplemented with 1% N2, 2% B27, basic fibroblast growth factor (10 ng/mL), human epidermal growth factor (20 ng/mL) and 0.4% relative humidity. Cells were fed or supplemented medium every 2 days unless passaged or extracted for use in *in vitro* assays.

CHLA20 human neuroblastoma cells (a gift from Mario Otto) were maintained in Dulbecco's Modified Eagle Medium high glucose (Gibco, Thermo Fisher Scientific) supplemented with 10% fetal bovine serum (Gibco, Thermo Fisher Scientific) and 1% penicillin–streptomycin. Cells were fed or supplemented medium every 2 days unless passaged or extracted for use in impedance assays.

Naïve healthy donor T cells (HF24W) were isolated from whole blood and established in culture according to procedures approved by the University of Georgia Institutional Review Board protocol (IRB ID: MOD00008066). H24FW T cells were maintained in ImmunoCult-XF T cell Expansion Medium (STEMCELL Technologies, Cambridge, MA, USA) and were fed with medium every 2 days unless passaged or extracted for use in *in vitro* assays. At 24 h before use in co-culture impedance assays, T cells were activated with ImmunoCult CD3/CD28 Activation Serum (STEMCELL Technologies). Cells were incubated at 37°C, 5% CO_2.

T cells were originally isolated from healthy donors as approved by the institutional review board of the University of Wisconsin-Madison (#2018-0103) and established in culture as described previously [33]. Bulk T cells were cultured in ImmunoCult-XF Expansion Medium before stimulation and subsequent electroporation (VFC CAR-T or VFC mCherry) or spinoculation (RV CAR-T) to insert the CAR transgene (pSFG.iCasp9.2A.14G2A-CD28-OX40-CD3z, a gift from Malcolm Brenner) as described elsewhere [33]. GD2 RV and VFC CAR T cells produced at University of Wisconsin-Madison by one donor were frozen in 90% fetal bovine serum + 10% dimethyl sulfoxide at 10 million cells/vial and shipped on dry ice to University of Georgia for use in these studies. GD2 CAR T cells were thawed briefly in a 37°C water bath and transferred into fresh ImmunoCult basal media with ImmunoCult CD3/CD28 Activation Serum for expansion before use in assays.

Co-culture assays for impedance measurement

For impedance measurement in the Axion Maestro platform using patient-derived GSCs, each 96-well impedance plate (Axion Biosystems, Atlanta, GA, USA) was prepared by coating with 0.05% polyethylenimine, followed by 20 μg/mL laminin overnight at 37°C. Assays using CHLA20 neuroblastoma cells did not require coating before use. After coating was complete, wells were rinsed thrice with

deionized water and then overlaid with 100 μL of cell culture media. The plate was placed into the analyzer to record baseline readings of the background impedance without cells present. After a baseline was established, the plate was removed from the analyzer and was seeded with 50 000 GSCs in a volume of 200 μL/well. After cell plating, the plate was left in the cell culture hood for 1 h at room temperature to ensure settling and attachment of the cells down to the microelectrodes on the bottom surface. The plate was then returned to the analyzer for data collection. Data were collected every 1 min for 48 h for cell monolayer growth measurement. For T-cell co-culture assays, data collection was briefly paused at 48 h, and the media was replaced with 200 μL of media containing either dosages of T cells or media alone. The plate was returned to the analyzer and data acquisition resumed 200 μL of media was replaced every 48 h over a period of 7 days. Changes in impedance are reported as the resistive component of the complex impedance, which is similar to quantifications described previously [34–36]. Using AxIS Z software (Axion BioSystems), all data are corrected for "media alone" to remove any changes in media only impedance over time. Data were then normalized to the impedance at the time of addition of effector cells. The % cytolysis calculations use the "target cell alone" (i.e., no treatment control) and "full lysis" controls to determine % of target cell cytolysis at every collected time point as follows:

$$\%Cytolysis_{sample}(t) = \left[\frac{Z_{sample}(t) - Z_{FullLysis}(t)}{Z_{TargetOnly}(t) - Z_{FullLysis}(t)}\right] x\ 100\%$$

Imaging and flow cytometry

Patient GSCs were labeled with fluorescently conjugated antibodies against GD2, CSPG4, CD133/1 and EGFR (Table 1) to quantify expression of CAR T-cell target antigens using imaging flow cytometry. GSCs were stained in FACS buffer (1X phosphate-buffered saline supplemented with 2% fetal bovine serum) and then events were acquired using the Amnis ImageStreamX MarkII imaging cytometer (Luminex Corporation, Austin, TX, USA) for analysis using the IDEAS software (Luminex Corporation).

Healthy donor H24FW T cells or GD2 CAR-T cells cultured in ImmunoCult medium (STEMCELL Technologies) or recovered from GSC impedance assays were collected after 96 h and labeled with fluorescently conjugated antibodies against CD3, CD4, CD8, CD69, CD137, PD-1, LAG3 and TIM3 (see Table 1). CAR was detected using 1A7 anti-14G2a isotype antibody (Biological Resources Branch, National Cancer Institute, Bethesda, MD, USA) conjugated to APC using a Lightning-Link APC Antibody Labeling kit (Novus Biologicals, Littleton, CO, USA). T cells were stained in fluorescence-activated cell sorting buffer and then flow cytometry was performed on an NovoCyte Quanteon flow cytometer (Agilent Technologies, Santa Clara, CA, USA) before data analysis using FlowJo 10.7.1 software (Becton Dickenson, Franklin Lakes, NJ). The live/dead Zombie Yellow Fixable Viability Kit (BioLegend, San Diego, CA, USA) was used to exclude dead cells, and populations of interest were identified after gating for: live, size, forward and side scatter, and then CD3+ cells.

Table 1
Antibodies used in flow cytometry, immunocytochemistry and immunohistochemistry.

Name	Company	Catalog number
Zombie Yellow	BioLegend	423103
CD133/1	Miltenyi Biotec	130-113-108
EGFR	BioLegend	352918
GD2	BioLegend	357308
CSPG4	eBioscience	53-6504-82
CD3	BioLegend	300470
CD4	BD Biosciences	561840
CD8a	BioLegend	300908
CD69	BioLegend	310930
CD137	BioLegend	745079
PD-1	BioLegend	367425
LAG-3	BioLegend	369307
TIM3	eBioscience	25-3109-41
CD3	BioLegend	300402
CC3	Cell Signaling	9661S

Cytokine assessment

Media samples were collected at every media change during impedance assays and then immediately flash frozen on liquid nitrogen and stored in −80°C. Then, 100 μL samples were shipped on dry ice to Eve Technologies (Eve Technologies Corp., Calgary, Alberta, Canada) for analysis using the MILLIPLEX Human Cytokine Array Proinflammatory Focused 13-Plex Discovery Assay (MilliporeSigma, Burlington, MA, USA) performed using the Luminex 200 system (Luminex Corporation) according to manufacturer's protocol.

NMR metabolomics analysis of media samples

For two independent co-culture experiments, 50 μL of media was collected from each culture well at each time point, flash-frozen in liquid nitrogen and stored at −80°C. Samples were transported to the CCRC facilities on dry ice for NMR analysis. Run order of samples was randomized. Samples were prepared in two batches for each rack of NMR samples to be run. For each rack, samples were removed and sorted on dry ice, then thawed at 4°C for 1 hour. Samples were then centrifuged at 2990*g* at 4°C for 20 min to pellet any cells or debris that may have been inadvertently collected with the media. Then, 5 μL of 100/3 mM DSS-D6 in deuterium oxide (Cambridge Isotope Laboratories, Tewksbury, MA, USA) was added to 1.7-mm NMR tubes (Bruker BioSpin, Billerica, MA, USA), followed by 45 μL of media from each sample that was added and mixed, for a final volume of 50 μL in each tube. Samples were prepared at 4°C and in predetermined, randomized order. The remaining volumes from each sample (~4 μL) was combined to create an internal pool. This material was used for internal controls as well as metabolite annotation.

NMR spectra were collected on a Bruker Avance III HD spectrometer at 600 MHz using a 5-mm TXI cryogenic probe and TopSpin software (Bruker BioSpin). One-dimensional spectra were collected on all samples using the noesypr1d pulse sequence under automation using ICON NMR software. Two-dimensional HSQC and TOCSY spectra were collected on internal pooled control samples for metabolite annotation. One-dimensional spectra were manually phased and baseline corrected in TopSpin. Two-dimensional spectra were processed in NMRpipe [37]. One-dimensional spectra were referenced, water/end regions removed and normalized with the PQN algorithm [38] using an in-house MATLAB toolbox (The MathWorks, Inc., Natick, MA, USA). Raw and processed data and relevant processing scripts are available on Metabolomics Workbench (https://github.com/artedison/Edison_Lab_Shared_Metabolomics_UGA) [39].

Two-dimensional NMR spectra collected on pooled samples were uploaded to COLMARm web server [40], where HSQC peaks were automatically matched to database peaks. HSQC matches were manually reviewed with additional two-dimensional and proton spectra, as well as using GISSMO mixture simulation [41,42] to confirm the match. Annotations were assigned a confidence score based upon the levels of spectral data supporting the match as previously described [43]. Annotated metabolites were matched to non-overlapped features in processed 1D spectra and integrated using an interactive MATLAB script to obtain quantitative values. These values were batched corrected between the two independent experiments using the ComBat method implemented in MetaboAnalyst web server [44,45]. Fold changes of batch corrected metabolite abundances were then calculated relative to control media. These values were used for

subsequent standalone statistical analysis implemented in MetaboAnalyst, as well as predictive modeling.

Immunocytochemistry for T-cell–mediated apoptosis in GSC spheroids

In total, 50 000 target GSCs were plated into 96-well spheroid plates and left to aggregate for 48 h. Effector cells were plated at 1:1 ratio and left in co-culture for 48 h. At endpoint, spheroids were removed from culture for 4% paraformaldehyde fixation and then embedded in OCT for sectioning. Cryosections were acquired at 10-μm thickness using a cryostat (Leica Biosystems, Buffalo Grove, IL, USA) onto charged glass slides for subsequent staining with CD3, cleaved caspase-3 (CC3), GD2 and DAPI (Table 1). Images were acquired using a Zeiss LSM 710 confocal microscope equipped with Zen software (Carl Zeiss, Oberkochen, Germany). Quantification for T-cell infiltration into spheroids, and amount of CC3+ and GD2+ GSCs was performed using Volocity 6.3 software (PerkinElmer, Waltham, MA, USA).

Regression analyses for predictive modeling

Symbolic regression was performed using Evolved Analytics' DataModeler software (Evolved Analytics, Rancho Santa Fe, CA, USA). DataModeler uses genetic programming to create symbolic regression models and selects for the fittest models defined as those with the best trade-off of greatest accuracy (R^2 value) and lowest complexity as identified by a pareto front. The collection of the fittest models forms ensembles, where the models in the ensemble agree at observed data points but diverge in extrapolated parameter spaces to provide a trust metric. Models considered for ensemble inclusion were processed to ensure all top-level additive terms passed an analysis of variance (ANOVA) test of $P < 0.005$, as well as an interval arithmetic test to ensure no singularities within the nominal variable ranges. Feature selection was achieved by looking at which variables are present within the candidate models. Graphics and tables were generated by DataModeler.

In this analysis, DataModeler's SymbolicRegression function was used to develop algebraic models. The fittest models were analyzed to identify dominant variables using the VariablePresence and VariableCombinations functions. CreateModelEnsemble was used to define trustable models using selected variable combinations and these were evaluated using the ModelSummaryTable to identify key statistical attributes with prediction and residual performance assessed visually via the EnsemblePredictionPlot and EnsembleResidualPlot functions, respectively. The ResponsePlotExplorer and ResponseComparisonExplorer functions were used to examine interactive effects and the MultiTargetResponseExplorer was used to examine the impact of common variables for multiple responses.

Statistical analysis

All analyses for direct mean comparisons of E:T impedance responses, cytokine analyses and immunocytochemistry were performed using Student's *t*-tests and one-way ANOVAs for significance with appropriate post hoc tests using GraphPad Prism, version 9.0 (GraphPad, San Diego, CA, USA). Metabolite changes between co-culture groups were tested for significance with one-way ANOVA, and Tukey post-hoc test to identify significant comparisons, using MetaboAnalyst.

Results

Real-time profiling of GSC adherence, expansion, and T-cell–mediated cytolysis using cellular impedance

To determine the optimal seeding density for impedance cytotoxicity assays, patient-derived N08 GSCs were seeded within a range of 10 000–100 000 cells/well of a 96-well impedance assay plate for 48 h [9–11] before co-culture with a fixed ratio of 10:1 activated healthy donor T cells (H24FW) to N08 GSCs. GSC cell death resulting in reduction of impedance magnitude was observed at 48 h post-seeding across all seeding densities tested (see supplementary Figure 1A,B). Different ratios of activated H24FW T cells cocultured with GSC monolayers seeded at a fixed, 50 000 cell density indicated T-cell ratio–dependent non-specific cytotoxicity as indicated by corresponding changes in cellular impedance (see supplementary Figure 1C). The addition of T cells or CAR T cells alone had impedance signatures below lysis only controls; therefore, any observed impedance changes within co-cultures were believed to result from antigen-dependent recognition and cytotoxicity by RV or VFC CAR T cells (see supplementary Figure 1D,E).

GD2 is highly expressed in patient-derived GSCs

GD2 is a promising target for CAR T-cell therapy of GBM and has demonstrated potent anticancer activity in other solid tumors [46,47]. To determine whether anti-GD2 CAR T cells would be relevant effectors for use in GBM impedance cytotoxicity assays, we performed imaging flow cytometry on N08 GSCs along with other highly expressed cell surface antigens including GD2, CSPG4, CD133/1, and EGFR. Results indicated that GD2 and CSPG4 were the most abundantly expressed antigens and were significantly overexpressed when compared to CD133/1 and EGFR in N08-30 GSCs (Figure 1A). GD2 however, had a significantly greater mean fluorescence intensity compared with all other antigens tested (Figure 1B).

Differently engineered GD2 CAR T products demonstrate significant differences in real-time cytolysis kinetics but not in endpoint cytolysis

Three different CAR T-cell products were included in cell impedance cytotoxicity assays to determine differences in cytolysis kinetics and endpoint cytolysis. These included anti-GD2 RV CAR T, anti-GD2 VFC CAR T and VFC mCherry CAR T (mCh or mCherry) cells. The VFC mCherry CAR T cells contain the same disruption of the *TRAC* locus as the anti-GD2 CAR T cells but with a signaling-inert mCherry fluorescent protein instead of a CAR domain. These three CAR T-cell products were cocultured with N08-30 GSCs in 96-well cell impedance plates at 0.1, 1 and 10:1 E:T ratios, and impedance readings were continuously acquired for 7 d *in vitro*. At the 7-d experiment endpoint, gross cytotoxicity was calculated as a function of the reduction in impedance as described within the Methods section, which was found to be similar between the two anti-GD2 CAR T cells across all E:T ratios tested. No significant GSC cytotoxicity was observed in VFC mCherry control-treated wells (Figure 2A). Although endpoint cytolysis values were found to be similar between the RV and VFC-treated GSCs after 7 d of co-culture (Figure 2B), statistically significant differences in KT50 values between VFC and RV CAR T-cell treatments were observed across all E:T ratios tested (Figure 2C), indicating a faster rate of GSC cytolysis by VFC CAR T cells when compared with RV CAR T cells.

CAR T cells cocultured with GSCs demonstrate significant differences in activation and exhaustion markers

CAR T cells were cryopreserved in the vapor phase of liquid nitrogen until use in impedance assays. After thawing and pre-activation with the ImmunoCult Human CD3/CD28/CD2 T Cell Activator system (STEMCELL Technologies), a subset of cells was removed immediately for testing post-thaw viability. All CAR T-cell subsets demonstrated comparable levels of post-thaw viability greater than 70% as detected using Zombie Yellow staining (see supplementary Figure 2A) and revealed no statistically significant differences in cell proliferation as measured by fold change increase over the first 48 h in culture after

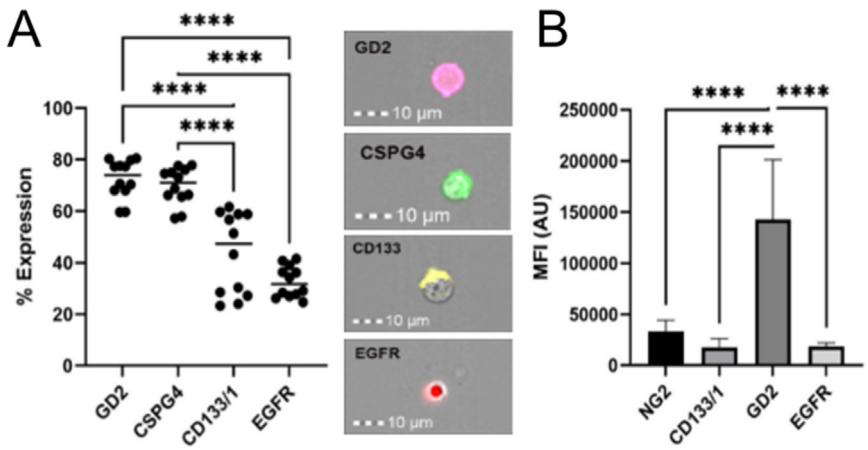

Fig. 1. GD2 is highly expressed in patient-derived GSCs. (A) ImageStream analysis of tumor-associated antigens on N08 GSCs. Representative merged brightfield and fluorescent images of GD2, CSPG4, CD133 and epidermal growth factor receptor (EGFR) collected via imaging cytometry. Quantifications represent 12 separate acquisitions of 1×10^5 events. Error bars represent mean ± standard deviation. $^*P < 0.05$, $^{**}P < 0.01$, $^{***}P < 0.001$ and $^{****}P < 0.0001$ determined by one-way ANOVA with post-hoc Tukey test. (B) ImageStream files were further analyzed for mean fluorescence intensity (MFI) values across positive cells for each marker. N = 12 for each marker. Error bars represent mean ± standard deviation, determined by one-way ANOVA with post-hoc Tukey test. (Color version of figure is available online.)

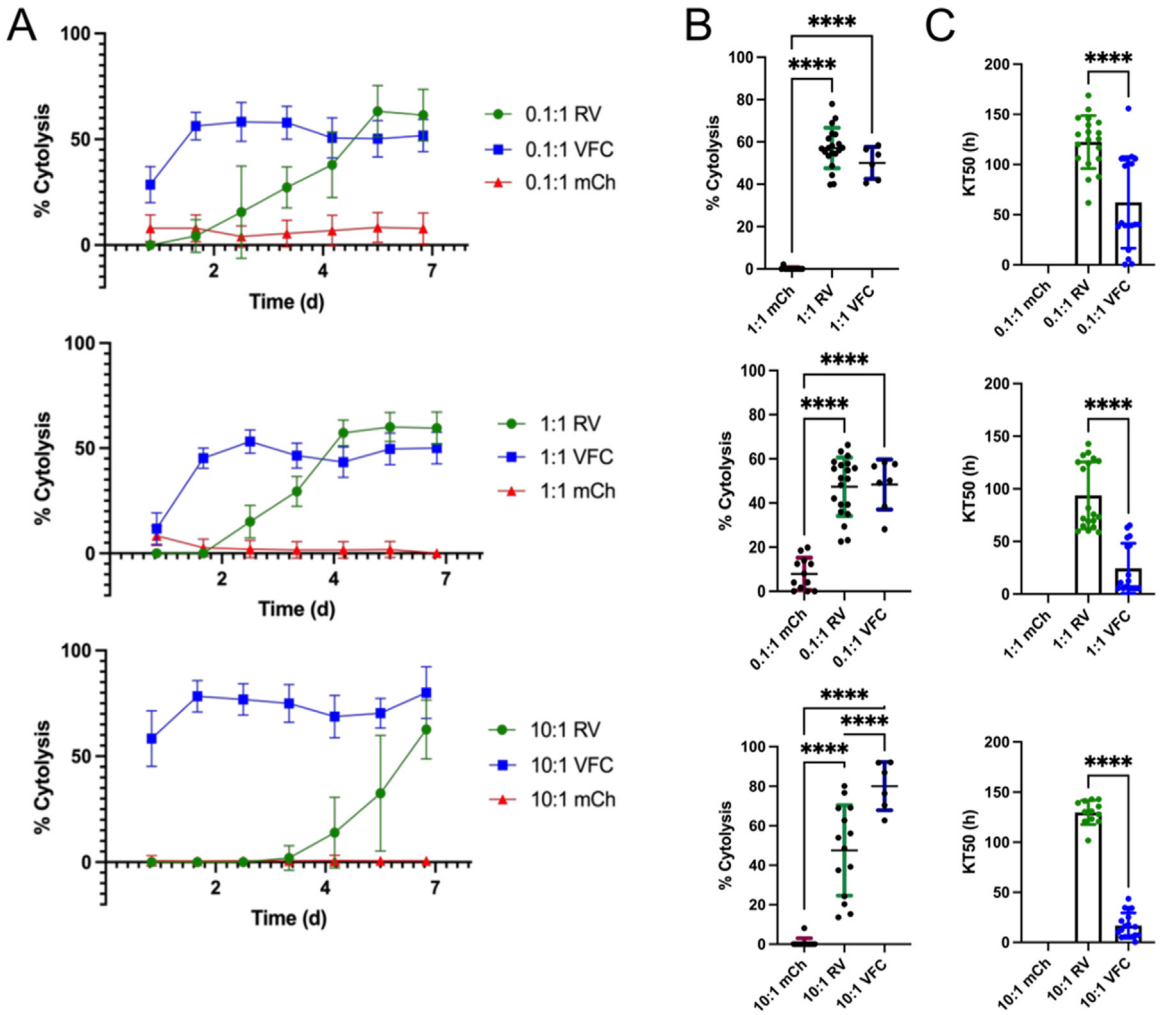

Fig. 2. Impedance assays demonstrate equal GSC killing ability at 7-day endpoint but reveal differential cytolysis kinetics between RV and VFC CAR T-cell products. (A) Cytolysis values plotted over time across mCh, RV and VFC-treated GSC monolayers. Plotted values are obtained from four experimental replicates containing 10–12 technical replicates each. (B) Percent cytolysis values were derived from target cell alone and full lysis control curve data. Percent cytolysis values at 7-day impedance assay endpoint shown across the comparative E:T ratios for VFC mCh, RV CAR T-cell and VFC CAR T-cell products. N = 12 for VFC mCh, N = 24 across RV and VFC CAR T-cell treatments. Error bars represent mean ± standard deviation. $^*P < 0.05$, $^{**}P < 0.01$, $^{***}P < 0.001$ and $^{****}P < 0.0001$ determined by one-way ANOVA with post-hoc Tukey test. (C) KT50 values were computed by AxIS Z software using no treatment baseline and lysis control curve data. N = 12 for VFC mCh, N =24 across RV and VFC CAR T-cell treatments. Mean values reported herein appropriate data set. Error bars represent mean ± standard deviation, determined by one-way ANOVA with post-hoc Tukey test. (Color version of figure is available online.)

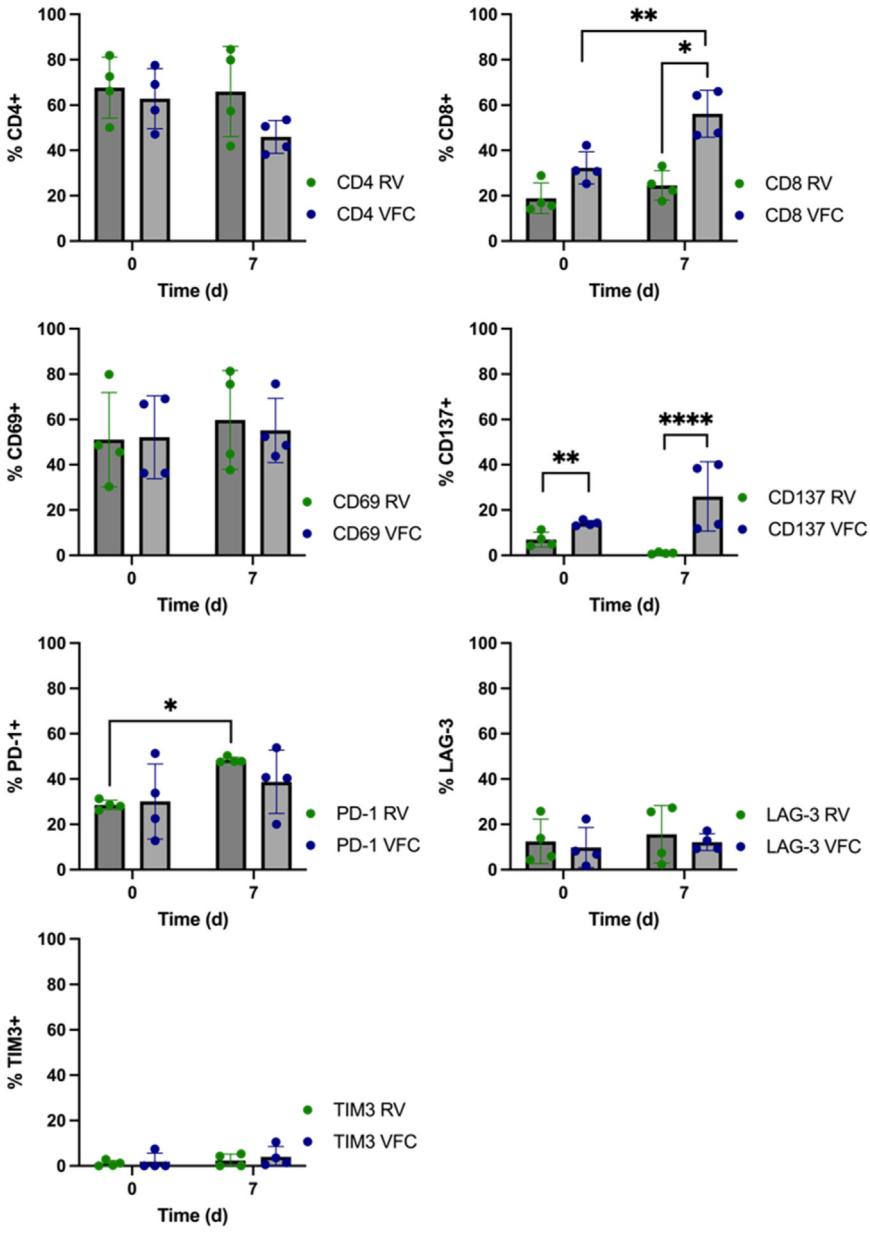

Fig. 3. VFC products display increased CD8+ cytotoxic lymphocyte populations and increased CD137+ activation in response to co-culture with GD2+ GSCs, compared with the maintenance of helper CD4+ populations and increased early exhaustion marker PD-1+ within RV products. Bar plots depicting flow cytometry data for time-matched RV and VFC CAR T cells within four repeated impedance experiments over 7 days of co-culture with GD2+ GSCs. All flow cytometry acquisitions represent 1×10^6 events. N = 4 across RV and VFC CAR T-cell treatments. Error bars represent mean ± standard deviation. $^*P < 0.05$, $^{**}P < 0.01$, $^{***}P < 0.001$ and $^{****}P < 0.0001$ determined by two-way repeated-measures ANOVA. (Color version of figure is available online.)

thawing (see supplementary Figure 2B). We detected significant differences in CAR+ cell numbers 48-h post-thaw, with RV CAR T cells demonstrating significantly more CAR+ T cells (57.4% in RV CAR T cells compared with 21.9% in VFC CAR T cells) (see supplementary Figure 2C). These changes reflected the greater efficiencies of gene transfer by RV before cryopreservation [32]. At baseline (see supplementary Figure 3A), both RV and VFC CAR T cells demonstrated a high number of CD69+ cells (~50%), indicating T-cell activation, presumably from pre-activation in the post-thaw culture conditions (Figure 3). A subset of VFC CAR T cells also expressed significantly greater levels of the activation marker CD137 before coculture with GSCs (Figure 3). Although the initial presence of PD-1 was observed in both RV and VFC CAR T cells before co-culture with GSCs, neither group contained greater than 10% of cells expressing LAG-3 or TIM3 exhaustion markers (Figure 3).

Within the first 48 h of coculture with GSCs, we detected significant increases in the amount of CD8+ T cells present in VFC CAR T cells that were recovered from GSC co-culture, compared with RV and pre-assay VFC CAR T cells (Figure 3). Both RV and VFC populations retained high CD69+ activation marker expression after 7 days in co-culture, but there was a significant increase in CD137+ activation as well in VFC CAR T cells compared with RV CAR T cells (Figure 3). There were no significant differences in PD-1+ expression between RV and VFC CAR T-cell populations after co-culture, but there was a significant increase in PD-1+ RV CAR T cells between the start of assay and 7 d in culture. At the 7-d experiment endpoint, there were no significant differences in the distribution of LAG-3+ or TIM3+ populations in RV and VFC CAR T cells, either between groups or compared with their pre-assay populations (Figure 3).

CAR T-cell products exhibit differential release of proinflammatory cytokines and extracellular metabolites after coculture with GD2+ GSCs

To examine further the observed functional differences between RV and VFC CAR T cells, media was sampled before and during

impedance assays for analysis of secreted cytokines that are associated with a proinflammatory response. Cytokines in pooled media from CAR T-cell cultures were measured before CAR T-cell coculture with GD2+ GSCs in impedance assays. Both RV and VFC CAR T cells secreted granulocyte-macrophage colony-stimulating factor (GM-CSF), tumor necrosis factor (TNF)α, interferon (IFN)γ, interleukin (IL)-8 and IL-13 before antigen recognition ("RV pre" and "VFC pre"; Figure 4A,B), reflecting either activation from expansion or tonic signaling. After 48 h of exposure to GD2+ GSCs, pooled media from 10:1 E:T ratio wells were analyzed for the same proinflammatory cytokines ("RV 48h" and "VFC 48h"). After antigen stimulation, VFC CAR T cells secreted elevated levels of GM-CSF, IFNγ, IL-5, IL-6, IL-8, IL-13, MCP-1, and TNFα (Figure 4A,B). In comparison, RV CAR T cells demonstrated little-to-no changes in cytokine levels except for GM-CSF, IFNγ and IL-13 after antigen stimulation compared with the pre-antigen group (Figure 4A,B), indicating potential exhaustion.

^{1}H-NMR analysis of media samples taken at the same time points profiled changes to relative concentrations of metabolites within each coculture system to indirectly assess CAR T-cell function. A heatmap representing all annotated metabolite fold-changes indicates unique patterns in CAR+ cells cocultured with GSCs when compared with the CAR-mCherry or GSCs alone (Figure 4C, see supplementary Figure 4A). Media from all cocultures showed decreased alanine when compared with media from GSCs alone (Figure 4C). Significantly increased levels of pyruvate and glutamate were detected in media sampled from both CAR T cell/GSC cocultures compared with mCherry-treated and untreated GSC culture media. This was also accompanied by a decrease in alanine, glutamine, formate and glutamate in media from CAR T-cell/GSC cocultures. In particular, RV CAR T/GSC co-cultures exhibited significantly reduced glutamine, formate and ethanol in media after 48 h of coculture compared to media from mCherry/GSC cocultures and GSC-only controls (Figure 4D). Media from RV CAR T cell/GSC cocultures also showed significantly reduced glutamine when compared with VFC CAR T-cell/GSC cocultures.

CAR T cells cocultured with GSC spheroids corroborate findings from impedance assays

We conducted coculture assays to validate CAR T-cell–induced cytotoxicity against three-dimensional GSC spheroids. GSC spheroids formed from an initial seeding density of 50 000 cells were cocultured at a 1:1 ratio with RV or VFC CAR T cells for 48 h before fixation and embedding for sectioning and immunostaining. After 48 h, GSC spheroids treated with VFC CAR T cells contained significantly less total GSCs remaining, and a significantly greater percentage of those remaining were found to be positive for the apoptosis marker CC3+ when compared with GSC spheroids treated with RV CAR T cells (Figure 5B,E). This increased cell death was accompanied by a greater number of total CD3+ VFC CAR T cells detected within spheroids at endpoint (Figure 5C), accompanied by a reduction in GD2+ GSCs found in both treated spheroid groups (Figure 5D). Together, these results further validate findings from impedance-based CAR T-cell potency assessment.

Impedance cytotoxicity assays against GD2+ CHLA20 neuroblastoma cells

To probe whether differential CAR T-cell performance was related to tumor cell specific interactions, the two CAR T-cell products (RV or VFC) were cocultured with GD2+ CHLA20 neuroblastoma cells in 96-well impedance plates at E:T ratios ranging from 0.1:1, 1:1 or 10:1 and impedance readings were acquired after 5 days of coculture. GD2 antigen density on CHLA20 cells was assessed as described previously for N08-30 GSCs using flow cytometry. Results indicated that CHLA20 neuroblastoma cells demonstrated a lower GD2+ population (70%) when compared with GSCs (90%) (see supplementary Figure 3C). Over the course of 4-d impedance assays, we found initial faster cytotoxicity by RV CAR T at 1:1 and 10:1 E:T ratios compared with the VFC CAR T-cell–treated CHLA20 cells (see supplementary Figure 5A), although endpoint cytotoxicity was found to be similar between the two anti-GD2 CAR T-cell treatments across all E:T ratios tested (see supplementary Figure 5B).

No significant differences in cytolysis were detected at subsequent timepoints or in other E:T ratios tested (i.e., 0.1:1, 10:1), with both RV and VFC CAR T cells performing equally over time (see supplementary Figure 5B).

Immunophenotyping of CAR T cells recovered from CHLA20 impedance assays demonstrated increased CD69+ RV CAR T cells (47%) compared with VFC (19%) at endpoint (see supplementary Figure 5C). Finally, media sampled from CAR T/CHLA20 cocultures was pooled and analyzed for proinflammatory cytokines. Within 48 h of co-culture with CHLA20 cells, RV CAR T cells released significantly greater amounts of GM-CSF, IFNγ, IL-8. MCP-1 and TNFα when compared with VFC CAR T cells, coinciding with increased cytolysis observed within the first 24 h (see supplementary Figure 5D).

Data integration and predictive modeling analyses indicate increased TNFα release and reduced glutamine, lactate and formate as predictive markers of CAR T-cell potency against N08 GSCs

We inputted the experimental outcomes into DataModeler software to determine predictive markers of RV or VFC CAR T-cell cytotoxic potency. DataModeler evolves hundreds to thousands of symbolic regression models and uses the fittest models (with the highest accuracy (R^2) and lowest complexity as determined using a Pareto front) and creates ensembles to identify leading parameters and parameter combinations which capture prediction and uncertainty. Machine learning and DataModeler software specifically have been used recently to predict and optimize critical quality parameters from multiomics data of cell therapy production [48,49]. Using symbolic regression, we examined interactive effects of cytokine and metabolite presence in media after 48 h in co-culture with GSCs to predict cytolysis happening at either the same time point, or to predict cytolysis at the assay endpoint. We found that 48-h TNFα levels were dominantly predictive of 48-h cytolysis outcomes, as seen in the variable combination matrix and associated ensemble plot demonstrating the influence of 48-h TNFα as an input parameter (Figure 6A,B). When we examined variable contributions for endpoint 7-day cytolysis, 48-h TNFα release continued to be a top contributor and was associated with reduced presence of metabolites glutamine, lactate and formate also at 48 h (Figure 6C,D). When we fit model ensembles to 7-day cytolysis, we found that increased cytotoxicity was strongly correlated to increasing concentrations of TNFα within 48 h of co-culture (Figure 6D). Conversely, increased endpoint cytotoxicity was correlated with decreasing amounts of glutamine, lactate, and formate in media sampling at the same 48-h time point (Figure 6D). As the 48-h TNFα release remained a dominant predictive input for both time points, we isolated the contributions of early 48-h TNFα release to 48-h cytolysis or 7-day endpoint cytolysis separated by treatment group as seen in the multi-response plots (Figure 6E). For both RV and VFC CAR T-cell–treated groups, similar curves demonstrate that early TNFα release is a stable predictor of observed effector CAR T-cell cytolysis against GSCs at both 48-h and 7 days' *in vitro* (Figure 6E).

Discussion

In this study, we investigated the potential of cellular impedance sensing as a tool for label-free, real-time assessment of CAR T-cell–mediated cytolysis of patient-derived GSCs. We observed differential cytolysis of GD2+ GSCs and CHLA20 neuroblastoma cells by two anti-GD2 CAR T cell products across a range of E:T ratios tested.

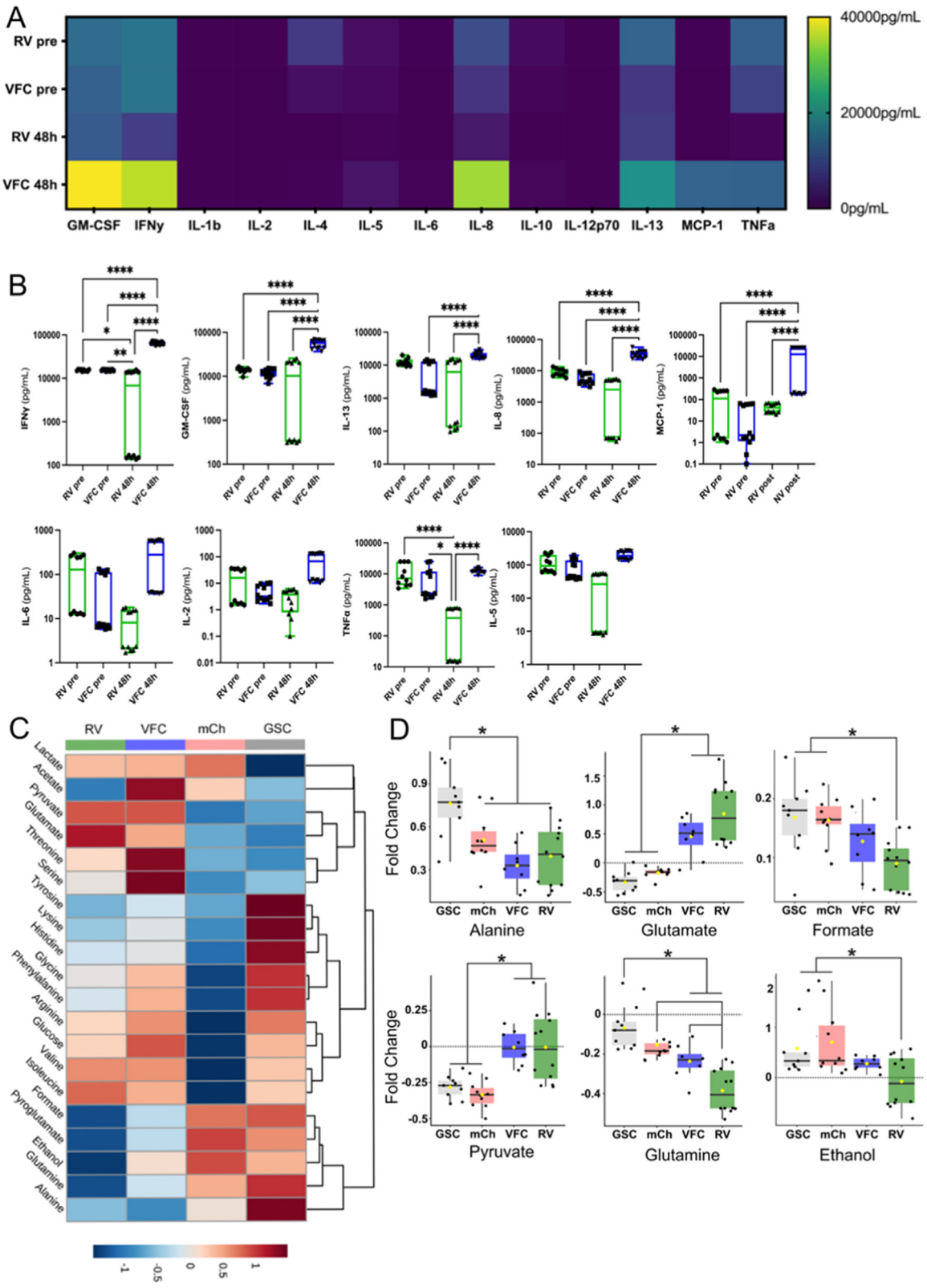

Fig. 4. RV products exhibit significantly reduced cytokine release after exposure to GSCs and altered metabolite fingerprint when compared with untreated GSCs or VFC products. (A) Cytokine production from conditioned pooled media taken from CAR T-cell products in culture pre- or post-antigen exposure. Post-antigen analysis contains pooled media samples after 48-h co-culture of RV and VFC CAR T-cell products with target GD2+ N08-30 GSCs. Values represent individual samples from pooled media in pg/mL concentrations, RV CAR T (N = 12) and VFC CAR T (N = 12) from two separate experiments. (B) Quantified cytokine values for individual pro-inflammatory cytokines found in pooled media samples from pre- or post-antigen exposure conditions between RV and VFC CAR T cells. Error bars represent mean ± standard deviation. $^{*}P < 0.05$, $^{**}P < 0.01$, $^{***}P < 0.001$ and $^{****}P < 0.0001$ determined by one-way ANOVA with post-hoc Brown-Forsythe test. (C) Individual media samples were also processed via NMR for metabolomics quantitation. Heatmap shown here of metabolite fold changes compared to media only control samples, 10:1 mCherry, 10:1 RV CAR T, 10:1 VFC CAR T. (D) Individual metabolites with significant differences in fold change of concentration across CAR T-cell treatments. Error bars represent mean ± standard deviation. $^{*}P < 0.01$ determined by one-way ANOVA with Tukey post-hoc test. (Color version of figure is available online.)

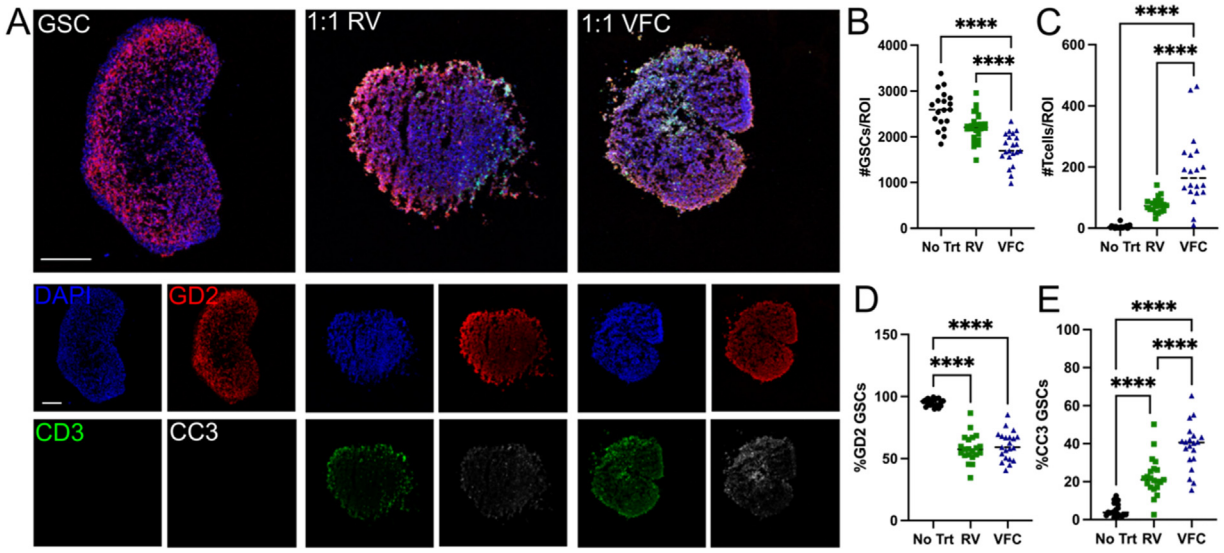

Fig. 5. VFC CAR T cells induce greater cytolysis of GD2+ GSC spheroids when compared with RV CAR T cells. (A) Representative confocal images of immunostained GSC spheroids after 48 h of co-culture with 1:1 RV CAR T or VFC CAR T cells compared with no treatment GSC spheroids alone. Spheroids were stained for DAPI, GD2, CD3 and CC3. Scale bar, 200 μm. Spheroid imaging was used to quantify GSC cell density within each spheroid, (C) an average number of T-cell infiltrates per spheroid, (D) difference in the percentage of GD2+ GSCs per spheroid across treatments and (E) percentage of CC3+ GSCs per spheroid at 48-h endpoint. N = 20. Error bars represent mean ± standard deviation. $^{****}P < 0.0001$ determined by one-way ANOVA with post-hoc Tukey test. (Color version of figure is available online.)

Impedance sensing has several advantages over conventional ^{51}Cr release assays, including the ability to perform real-time label-free analysis without radioactive isotopes while facilitating additional downstream analyses for potency assessment [50,51]. This is important for detecting cytotoxicity when the onset of killing might be delayed due to low E:T ratios or potential low-affinity T-cell interactions. Both are conditions that are hard to measure with ^{51}Cr release but important to consider when translating cellular immunotherapies to the clinic.

Impedance assessments provided real-time kinetics, which combined with flow cytometry, cytokine, and metabolite analysis of media samples, were used to uncover temporal changes in CAR T-cell potency against two different GD2+ tumor cells, GBM and neuroblastoma. We could detect impedance changes implicating significant cytolysis of both GD2+ GSCs and CHLA20 cells within 24 h in E:T ratios as low as 0.1:1 and were able to measure delayed or slower cytotoxicity over a period of 220 h. Anti-GD2 VFC CAR T cells demonstrated significantly increased rates of cytolysis of GD2+ GSCs compared with RV CAR T cells, which demonstrated the differential presence of T-cell activation markers and a lack of inflammatory cytokine release. Impedance assay results were further supported by results from three-dimensional GSC spheroid cocultures with anti-GD2 CAR T-cell products, which also revealed increased cytolysis of GSC spheroids by VFC CAR T cells in comparison with RV CAR T cells. Flow cytometry, cytokine, metabolite and spheroid assay results were used for predictive modeling analyses to identify markers of CAR T-cell potency against cancer cells, which can be used to determine critical quality attributes (CQAs) of CAR T- cell products in the Good Manufacturing Practices setting.

Virally transduced CAR T cells have demonstrated evidence of tonic signaling and emergence of premature anergic or exhausted cell phenotypes [27,52]. Non-viral CRISPR/Cas9 gene editing is more precise compared with retroviral gene integration methods in the ability to facilitate site-specific CAR insertion, such as under the transcriptional control of the *TRAC* promoter [27]. Concurrent TCR knockout and *TRAC*-regulated CAR expression enable complete CAR-based tumor cell recognition and potentially more efficient effector function, all without the constraints of MHC-limited recognition. When compared with GSC cytolysis by RV CAR T cells, which can be influenced by both CAR and TCR-mediated cytolysis, the near-complete TCR knockout in VFC CAR T cells signifies that VFC CAR T-cell cytolysis of GSCs was entirely CAR-mediated [33]. Before use in impedance assays, CAR T-cell products were thawed and activated using CD3/CD28 activation beads. No significant differences were observed in post-thaw viability, immediate proliferative ability, or in pre-assay cytokine release (see supplementary Figure 2A,B, Figure 4A,B). We quantified CAR+ cells in both RV and VFC CAR T cells tested post-thaw to ensure that there were no significant post-thaw changes compared to post-manufacturing quantifications (see supplementary Figure 2C). Although RV CAR T cells contained a greater number of CAR+ cells when compared with VFC CAR T cells post-thaw, these ratios were comparable to CAR+ cell numbers observed in the post-manufacturing, pre-cryopreservation assessment [32].

Label-free cell impedance sensing of CAR T-cell–induced GSC cytolysis indicated that the anti-GD2 RV CAR T cells demonstrated a significantly slower rate of cytolysis than VFC CAR T cells at all E:T ratios tested (Figure 2), despite having a significantly greater number of CAR+ cells than the VFC CAR T-cell population. These findings indicate that greater CAR gene transfer efficiency detected in the RV CAR T cells does not necessarily translate to more potent GSC cytotoxicity and that not all CAR+ cells in the RV CAR T-cell population may be functionally contributing to GSC cytotoxicity post-thaw. However, potency differences between differently engineered CAR T cells were reversed when RV and VFC CAR T cells from the same donor and manufacturing batch were used against GD2+ CHLA20 neuroblastoma cells (see supplementary Figure 5). Impedance cytotoxicity measurements using RV and VFC CAR T cells cocultured with GD2+ CHLA20 neuroblastoma cells indicated that when the same donor and manufacturing batch of CAR T cells were used, a rescue of RV CAR T cytotoxicity against CHLA20 neuroblastoma cells was observed, suggesting that impedance assays can discern between more or less potent E:T ratios between different donor cells or across different cancer types. It should be considered that the RV CAR T cells outperformed NV CAR T cells against CHLA20 due to variables including the retained TCR clonotypes within RV CAR T-cell populations, differences in secreted immunomodulatory cytokines between CHLA20 and GSCs or differentially preserved T-cell subsets within the CAR manufacturing methods. Studies with CAR T cells that retain

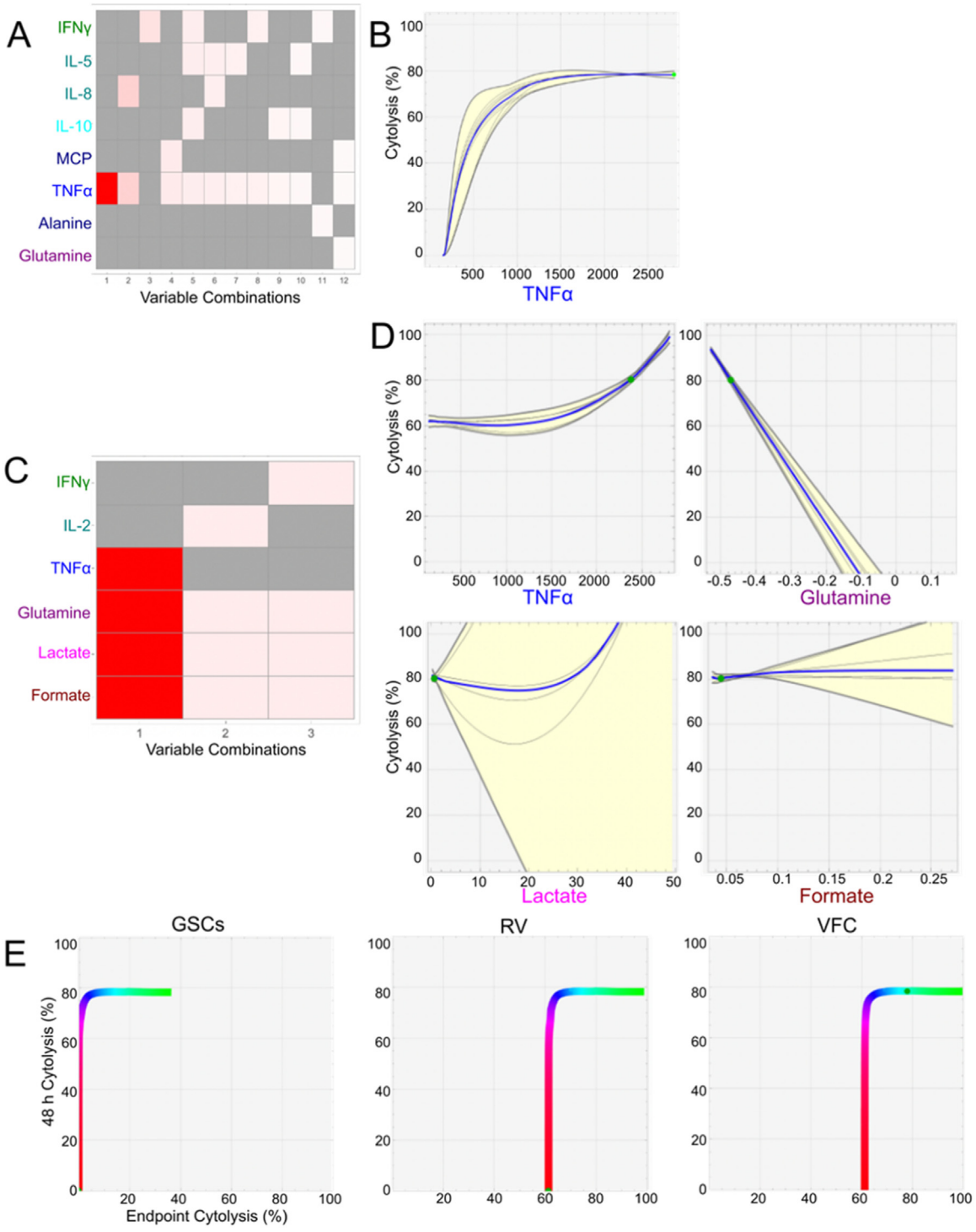

Fig. 6. TNFα alone and TNFα along with glutamine, lactate and formate are predictive of CAR T-cell potency at 48-h and 7-day endpoints, respectively. (A) Variable combination matrix for 48-h cytolysis shows that for both RV and VFC CAR T cells, function is predicted by TNFα release into media samples collected from impedance assays compared with any other metric at the same time points. (B) Associated ensemble plot showing response profile of 48 h cytolysis as a result of input parameter TNFα. Gray lines denote paths from a single given model within the ensemble, and the yellow area represents variation of the ensemble as a function of the parameter. (C) Variable combination matrix for 7-d cytolysis shows that for both RV and VFC CAR T cells, cytolysis is predicted by a combination of TNFα, glutamine, lactate and formate. (D) Ensemble plots showing response profiles of 7 d cytolysis as a function of input parameters TNFα, glutamine, lactate, and formate. (E) Multi-response plots comparing 48-h cytolysis and 7-d endpoint cytolysis (0%–100%) as a function of common variable TNFα concentration. Red is low level of TNFα, and green is high level of TNFα, as predicted by the model ensemble for each response. The green dot is the condition for a contributing data record within the appropriate group: GSCs alone, RV or VFC CAR T-cell treatment. (Color version of figure is available online.)

native TCRs should consider bulk TCR sequencing to identify expanded clones that contribute to additional cytotoxicity beyond CAR antigen recognition. Future works should involve multiple target tumor cell lines and multiple donor CAR T cells in a multiplexed pipeline to better interpret differences in cytolysis, involving additional parameters to measure relevant problems plaguing the translation of autologous cellular immunotherapies including target antigen heterogeneity, tumor microenvironmental immunosuppression,

variable quality on isolated donor cells, manufacturing processing and handling, and lack of manufactured cell persistence.

Davenport *et al.* [53] provide evidence for greater functional activity of CAR+ cells lacking a TCR, indicating that CAR+TCR+ CAR T cells could be inhibited by the presence of the TCR, which uses similar signaling molecules like CD3ζ. It has also been shown that differences in costimulatory domains and CAR insertion result in altered activation kinetics, receptor aggregation, and signaling, which is reflected in the time to lysis response [54,55]. The current methods for assessing *in vitro* functionality of CAR T-cell products do not reliably predict *in vivo* responses in animal models, let alone human trials, but parallel processing of potency assay markers such as time to lysis responses, cytokine or metabolite changes, and predictive modeling could help bridge those gaps. The differences in cytolysis of GD2+ GSCs observed in our studies may have stemmed from random CAR insertion and presence of native TCR in RV CAR T cells, or perhaps from the behavior of target GSCs within respective assays. However, the lack of observed differences in cytotoxicity between RV and VFC CAR T cell products cocultured with CHLA20 cells suggest that multifocal target cell contributions to these co-culture platforms also influence CAR T-cell potency beyond target antigen expression. Our findings suggest that cell impedance-based assessment of real-time kinetics of cytolysis by CAR T cells can help identify functional differences between CAR T-cell products by providing temporal resolution of activation and lysis.

Immunophenotyping of both RV and VFC CAR T cells suggest that they responded similarly to coculture with GD2+ GSCs, with both CAR T-cell products expressing a high number of CD69+ and few exhausted cells (LAG-3+, TIM3+) after 7 d in coculture with GSCs (Figure 3). Interestingly, while RV CAR T cell populations maintained a high number of CD69+ cells over 7 d of GSC exposure, VFC CAR T cells demonstrated a significantly greater presence of CD137+ cells that continued to increase over 7d in coculture (Figure 3). CD137 is expressed by tumor-infiltrating lymphocytes that show a stronger response to tumor antigens, acting as a potent costimulatory molecule for T cells and its function has been linked to T-cell persistence and expansion [55–59]. We speculate that the greater number of CD137+ VFC CAR T cells is likely responsible for antigen recognition and more potent anti-tumor activity against GD2+ GSCs, but exacting the mechanism underpinning the differential response we observed against GD2+ CHLA neuroblastoma cells was outside the scope of data within this study. The greater persistence of CD137+ activated VFC CAR T cells when compared with RV CAR T cells corroborates differences in cytolysis kinetics, suggesting that they possessed a significant functional advantage over RV CAR T cells (Figures 2 and 3). Although neither RV nor VFC CAR T cells demonstrated any premature expression of exhaustion markers before GSC coculture, a wide distribution of PD-1+ cells was detected in experimental replicates of both RV and VFC CAR T cells, with RV CAR T cells demonstrating a significant increase in PD-1+ cells after coculture with GD2+ GSCs (Figure 3). Increased PD-1+ RV CAR T cells, in combination with a lack of inflammatory cytokine release by RV CAR T cells within 48 h of antigen exposure to GD2+ GSCs, could support the observed lack of functional cytotoxicity by RV CAR T cells at early coculture timepoints and signal the shift from activation to exhaustion earlier than VFC CAR T cells (Figure 4). In contrast to results from coculture of CAR T cell products with GSCs, we found that RV and VFC CAR T cells produced from the same donor and manufacturing batch showed no significant differences in activation and exhaustion marker presence when cocultured with CHLA20 cells (see supplementary Figure 5), which corroborate comparable real-time and endpoint cytolysis of CHLA20 neuroblastoma cells by CAR T cell products across all E:T ratios tested.

Evidence of T-cell activation in both RV and VFC CAR T cells before GSC antigen exposure was confirmed by the presence of inflammatory cytokines in media (Figure 4A). Before antigen exposure, RV CAR T cells were found to release elevated amounts of IL-8, IL-13 and TNFα, reflecting activation due to the expansion method or tonic signaling of the CAR. However, the observed cytokine release by RV CAR T cells is completely diminished after antigen exposure, in contrast to the continued and enhanced cytokine release by VFC CAR T cells in co-culture with GSCs (Figure 4B). Attenuated proinflammatory cytokine release by RV CAR T cells along with the continued presence of highly activated cells corroborates decreased cytotoxic activity observed in impedance cytolysis assays. In contrast to findings from CAR T-cell/GSC cocultures, evidence from cytokine analysis of media from CAR T cell/CHLA20 cocultures confirmed enhanced RV CAR T anti-cancer activity in comparison to VFC CAR T cells within the first 48 h, in combination with elevated post-antigen exposure release of GM-CSF, IFNγ, IL-8, and MCP-1 (see supplementary Figure 5). Currently used CQAs in CAR T-cell manufacturing include short-term cytolysis and IFNγ release [56–62]. However, despite their use as potency indicators for CAR T-cell products, neither cytotoxicity nor IFNγ release alone are predictive of clinical efficacy and safety *in vivo* due to the complex features of CAR T cells and the tumor microenvironment [63,64]. Our secretome analyses not only found that differences in IFNγ release within co-cultures were linked to cytotoxicity, but also significantly implicated TNFα release in predicting tumor cytotoxicity of RV and VFC CAR T cells through additional predictive modeling. Like IFNγ, TNFα is also released during T-cell activation, and loss of TNF sensitivity in the tumor microenvironment has been implicated as a mechanism of tumor immune evasion [65,66].

Initiation of T-cell activation results in the rapid reprogramming of cellular metabolism towards increased one-carbon metabolism, glutaminolysis and glycolysis, in order to meet the biosynthesis demands of proliferation, differentiation and effector function [67–70]. Consumption of glutamine is implicated in T-cell activation, which is increased in both CAR T-cell products compared with GD2+ GSCs alone, but more so in RV when compared with VFC CAR T cells, corresponding to the differences in CAR+ and CD69+ populations between the two groups [71,72] (Figure 4C,D). The first product of glutamine metabolism is glutamate, which serves as a metabolic nexus to either amino acid or glutathione synthesis for T cell activation [73,74]. Formate is a byproduct of the one-carbon cycle that takes place in mitochondria, and may be a marker of increased central memory T-cell subpopulations [36]. Although we did not detect any statistically significant differences in formate production between RV and VFC CAR T-cell co-cultures, it is on average lower in RV, possibly reflecting less mitochondrial activity and CAR T-cell activity. Increased serine and glycine in conditioned media of VFC CAR T-cell cocultures may also reflect differential activity in the one-carbon cycle.

RV CAR T cells appear to broadly demonstrate increases in consumption of several metabolites compared to VFC CAR T cells (Figure 4C). This could result from the dual CAR+TCR+ cells in the RV CAR T cells responding to GD2+ GSCs, compared to the CAR+TCR- VFC CAR T cells. RV CAR T cells also demonstrated increased variability in metabolite profiles across multiple experimental replicates when compared with mCh and VFC CAR T cells, which could have resulted from variable CAR insertion when compared to targeted CAR insertion in mCh and VFC CAR T cells (Figure 4D).

Significant differences in pyruvate, glutamine and glutamate in CAR-TCR-mCherry CAR T cells indicate that CAR insertion plays an important role in the downstream activation and metabolic pathways of CAR T cells that could be impacting performance in functional cytotoxicity assays (Figure 4C,D). Multivariate principal component analysis of quantified metabolites demonstrates clustering based on CAR+ cells, reconfirming that successful CAR expression has lasting effects on the metabolism of engineered T cells that can translate to potency differences of CAR T-cell products (see supplementary Figure 4B).

It should be noted that the conditioned media profiles detected by cytokine release assays and NMR metabolite analyses are an

accumulation of all cellular activity in the culture, including the GSCs and different engineered T-cell products, which is why examining differences between co-cultures and controls is important for interpretation. In addition to the metabolic activity of the different T cell products, GSC metabolism, cytokines or metabolites released from GSC death, and total cell numbers present in the culture at sampling influence these media profiles. However, previous co-culture experiments have suggested that T-cell metabolism appears to dominate the observed changes in co-culture media profiles, so inferences can be made about the differential metabolic activity between different T-cell products. Taken holistically, our findings indicate that changes in the secretome including TNFα, glutamine, formate and glutamate in conditioned media from GSC coculture assays reflected differential CAR T-cell cytotoxicity outcomes. Lymphocyte metabolism is linked to antitumor response, and CAR T cells demonstrate altered metabolic programming when manufactured from different patient T-cell subsets or when manufactured using different co-stimulatory domains [75–77].

In addition to increased interest in CAR T-cell metabolism, there is increased urgency in understanding the impact of tumor-secreted immunomodulatory signals on CAR T-cell function. Ideally, potency assays will encompass a spectrum of these clinically relevant functions within a cellular therapy product as CQAs, as well as reflect patient-specific or microenvironment-specific markers for success. One assay alone is likely insufficient to measure potency of CAR T-cell therapies and will instead require multiple complementary assays that measure simultaneous characteristics associated with quality, consistency, and stability [78]. In an attempt to address this, we integrated results from impedance, immunophenotyping, cytokine, and metabolomics analyses and used nonlinear predictive modeling to derive CQAs of CAR T cell potency. This approach allowed us to compare the predictive capabilities of individual assays relative to the benefits of integrated datasets. Taking this approach, we found that 48-h cytokine levels and in particular, TNFα release, were most predictive of CAR T-cell cytotoxicity at 48 h (Figure 6A,B); whereas a combination of 48-h cytokines (TNFα) and 48-h metabolites (glutamine, lactate and formate) were most predictive of 7-d endpoint CAR T cell cytotoxicity (Figure 6C,D) for both RV and VFC CAR T cells. Furthermore, the results predict that the combination of high levels of TNFα release and low levels of glutamine, lactate and formate result in the highest level of endpoint CAR T-cell potency.

Sensitive, real-time assays to investigate E:T ratios, avidity of interaction and time to response are needed to identify reliable CQAs of cellular therapies for solid tumors. Manufacturing CAR T-cell products for patient use typically involves cryopreservation of the final product before use, and the impact of cryopreservation on CAR T-cell efficacy and characteristics is unclear. Cellular impedance changes induced by CAR T-cell cytolysis of cancer cells is a fast, sensitive assay for measuring cell killing, when compared to other *in vitro* platforms that rely on either destructive labeling, endpoint readouts, or less direct measurements of tumor cell viability. Assays measuring impedance-based lysis kinetics can explore CAR T-cell effector cell function, specificity and affinity to their target antigen, whereas additional inline methods can quantify other key attributes of potency in cellular immunotherapy products. A promising application of this impedance-based potency assessment system would be to evaluate differences across different donor CAR T-cell products or across many different patient-derived tumor cell lines to establish a baseline of CAR T-cell fitness that could screen for successful manufacturing or inform product release criteria after cryopreservation. These *in vitro* potency metrics can not only help us answer fundamental questions but could also aid in cell manufacturing workflow and decision-making. The ability to better characterize CQAs of cellular therapy products *in vitro* may increase the likelihood of predicting CAR T-cell *in vivo* responses for solid tumors.

Declaration of Competing Interest

KS is a member of the scientific advisory boards of Andson Biotech and Notch Therapeutics and receives research support from Synthego Corporation, Spotlight Therapeutics, and the Center for Cell Manufacturing Technologies. LK received in-kind contributions of assay consumables from Axion Biosystems Inc., and research support from the Center for Cell Manufacturing Technologies. SC is employed by Axion Biosystems Inc. TK is owner and employee of Evolved Analytics LLC., licensor of DataModelor.

Funding

We acknowledge funding from the American Brain Tumor Association (to LK), the MACC Fund (to CMC) and the NSF Engineering Research Center (ERC) for Cell Manufacturing Technologies (CMaT, NSF-EEC 1648035) (to CMC, KS, LK), the National Science Foundation (DGE-1747503) (to KM), National Institute of General Medical Sciences R35 GM119644-01 (to KS); the University of Wisconsin (UW)-Madison Office of the Vice Chancellor for Research and Graduate Education with funding from the Wisconsin Alumni Research Foundation, UW Carbone Cancer Center P30 CA014520, Hyundai Hope on Wheels and the Grainger Institute for Engineering at UW-Madison (to CMC and KS). The contents of this article do not necessarily reflect the views or policies of the Department of Health and Human Services, nor does mention of trade names, commercial products, or organizations imply endorsement by the US Government.

Author Contributions

Conception and design of the study: MTL, MC and LK. Acquisition of data: MTL, MC, DV, RR, CT, SC, HH and AE. Analysis and interpretation of data: MTL, MC, KM, NP, CMC, AD, KS, TK and LK. Drafting or revising the manuscript: MTL, MC, KM, NP, CMC, AD, KS, SC, HH, AE and LK. All authors have approved the final article.

Supplementary materials

Supplementary material associated with this article can be found in the online version at doi:10.1016/j.jcyt.2023.01.008.

References

[1] Gill S, Maus MV, Porter DL. Chimeric antigen receptor T cell therapy: 25years in the making. Blood Rev. 2016;30(3):157–67.
[2] Filley AC, Henriquez M, Dey M. CART immunotherapy: development, success, and translation to malignant gliomas and other solid tumors. Front. Oncol. 2018;8:453.
[3] Li J, et al. Chimeric antigen receptor T cell (CAR-T) immunotherapy for solid tumors: lessons learned and strategies for moving forward. J. Hematol. Oncol. 2018;11(1):22.
[4] Newick K, Moon E, Albelda SM. Chimeric antigen receptor T-cell therapy for solid tumors. Mol Ther Oncolytics 2016;3:16006.
[5] Bagley SJ, et al. CAR T-cell therapy for glioblastoma: recent clinical advances and future challenges. Neuro. Oncol. 2018;20(11):1429–38.
[6] Hardiansyah D, Ng CM. Quantitative systems pharmacology model of chimeric antigen receptor T-cell therapy. Clin Transl Sci 2019;12(4):343–9.
[7] Stein AM, et al. Tisagenlecleucel model-based cellular kinetic analysis of chimeric antigen receptor-T cells. CPT Pharmacometrics Syst Pharmacol 2019;8(5):285–95.
[8] Harris DT, et al. Comparison of T cell activities mediated by human TCRs and CARs that use the same recognition domains. J. Immunol. 2018;200(3):1088–100.
[9] Peper JK, et al. An impedance-based cytotoxicity assay for real-time and label-free assessment of T-cell-mediated killing of adherent cells. J. Immunol. Methods 2014;405:192–8.
[10] Lo CM, Keese CR, Giaever I. Impedance analysis of MDCK cells measured by electric cell-substrate impedance sensing. Biophys. J. 1995;69(6):2800–7.
[11] Rahman AR, et al. Cell culture monitoring by impedance mapping using a multi-electrode scanning impedance spectroscopy system (CellMap). Physiol. Meas. 2008;29(6):S227–39.
[12] Zhang Y, et al. Real-time monitoring of extracellular matrix-mediated PC12 cell attachment and proliferation using an electronic biosensing device. Biotechnol. Lett 2012;34(2):397–404.

[13] Lovelady DC, et al. Detecting effects of low levels of cytochalasin B in 3T3 fibroblast cultures by analysis of electrical noise obtained from cellular micromotion. Biosens. Bioelectron. 2009;24(7):2250–4.
[14] Opp D, et al. Use of electric cell-substrate impedance sensing to assess in vitro cytotoxicity. Biosens. Bioelectron. 2009;24(8):2625–9.
[15] Keese CR, et al. Electrical wound-healing assay for cells in vitro. Proc Natl Acad Sci U S A, 2004;101(6):1554–9.
[16] Keese CR, et al. Real-time impedance assay to follow the invasive activities of metastatic cells in culture. BioTechniques 2002;33(4):842–4. 846, 848-50.
[17] Heileman K, Daoud J, Tabrizian M. Dielectric spectroscopy as a viable biosensing tool for cell and tissue characterization and analysis. Biosens. Bioelectron. 2013;49:348–59.
[18] Xu Y, et al. A review of impedance measurements of whole cells. Biosens. Bioelectron. 2016;77:824–36.
[19] Giaever I, Keese CR. Monitoring fibroblast behavior in tissue culture with an applied electric field. Proc Natl Acad Sci U S A, 1984;81(12):3761–4.
[20] Giaever I, Keese CR. A morphological biosensor for mammalian cells. Nature 1993;366(6455):591–2.
[21] Wegener J, Keese CR, Giaever I. Electric cell-substrate impedance sensing (ECIS) as a noninvasive means to monitor the kinetics of cell spreading to artificial surfaces. Exp. Cell. Res. 2000;259(1):158–66.
[22] Wegener J, Keese CR, Giaever I. Recovery of adherent cells after in situ electroporation monitored electrically. BioTechniques 2002;33(2):348.. 350, 352 passim.
[23] Cerignoli F, et al. In vitro immunotherapy potency assays using real-time cell analysis. PLoS One 2018;13(3):e0193498.
[24] Piscopo NJ, et al. Bioengineering solutions for manufacturing challenges in CAR T cells. Biotechnol. J. 2018;13(2).
[25] Wang X, Riviere I. Clinical manufacturing of CAR T cells: foundation of a promising therapy. Mol Ther Oncolytics 2016;3:16015.
[26] Nobles CL, et al. CD19-targeting CAR T cell immunotherapy outcomes correlate with genomic modification by vector integration. J. Clin. Invest. 2020;130(2):673–85.
[27] Eyquem J, et al. Targeting a CAR to the TRAC locus with CRISPR/Cas9 enhances tumour rejection. Nature 2017;543(7643):113–7.
[28] Jinek M, et al. A programmable dual-RNA-guided DNA endonuclease in adaptive bacterial immunity. Science 2012;337(6096):816–21.
[29] McGuire AL, et al. The road ahead in genetics and genomics. Nat. Rev. Genet. 2020;21(10):581–96.
[30] Doudna JA. The promise and challenge of therapeutic genome editing. Nature 2020;578(7794):229–36.
[31] Sachdeva M, et al. Repurposing endogenous immune pathways to tailor and control chimeric antigen receptor T cell functionality. Nat. Commun. 2019;10(1):5100.
[32] Mueller KP, et al. Production and characterization of virus-free, CRISPR-CAR T cells capable of inducing solid tumor regression. J. Immunother. Cancer 2022;10(9):e004446.
[33] Mueller KP, et al. CRISPR-mediated insertion of a chimeric antigen receptor produces nonviral T cell products capable of inducing solid tumor regression. Cold Spring Harbor Laboratory; 2021.
[34] Scott CW, et al. An impedance-based cellular assay using human iPSC-derived cardiomyocytes to quantify modulators of cardiac contractility. Toxicol. Sci. 2014;142(2):331–8.
[35] Guo L, et al. Estimating the risk of drug-induced proarrhythmia using human induced pluripotent stem cell-derived cardiomyocytes. Toxicol. Sci. 2011;123(1):281–9.
[36] Peters MF, et al. Human stem cell-derived cardiomyocytes in cellular impedance assays: bringing cardiotoxicity screening to the front line. Cardiovasc. Toxicol. 2015;15(2):127–39.
[37] Delaglio F, et al. NMRPipe: a multidimensional spectral processing system based on UNIX pipes. J. Biomol. NMR 1995;6(3):277–93.
[38] Dieterle F, et al. Probabilistic quotient normalization as robust method to account for dilution of complex biological mixtures. Application in 1H NMR metabonomics. Anal. Chem. 2006;78(13):4281–90.
[39] Sud M, et al. Metabolomics workbench: an international repository for metabolomics data and metadata, metabolite standards, protocols, tutorials and training, and analysis tools. Nucleic. Acids. Res. 2016;44(D1):D463–70.
[40] Bingol K, et al. Comprehensive metabolite identification strategy using multiple two-dimensional NMR spectra of a complex mixture implemented in the COLMARm web server. Anal. Chem. 2016;88(24):12411–8.
[41] Dashti H, et al. Spin system modeling of nuclear magnetic resonance spectra for applications in metabolomics and small molecule screening. Anal. Chem. 2017;89(22):12201–8.
[42] Dashti H, et al. Applications of parametrized NMR spin systems of small molecules. Anal. Chem. 2018;90(18):10646–9.
[43] Walejko JM, et al. Global metabolomics of the placenta reveals distinct metabolic profiles between maternal and fetal placental tissues following delivery in nonlabored women. Metabolites 2018;8(1).
[44] Chong J, Wishart DS, Xia J. Using metaboAnalyst 4.0 for comprehensive and integrative metabolomics data analysis. Curr Protoc Bioinformatics 2019;68(1):e86.
[45] Johnson WE, Li C, Rabinovic A. Adjusting batch effects in microarray expression data using empirical Bayes methods. Biostatistics 2007;8(1):118–27.
[46] Nazha B, Inal C, Owonikoko TK. Disialoganglioside GD2 expression in solid tumors and role as a target for cancer therapy. Front. Oncol. 2020;10:1000.
[47] Salinas RD, Durgin JS, O'Rourke DM. Potential of glioblastoma-targeted chimeric antigen receptor (CAR) T-Cell therapy. CNS Drugs 2020;34(2):127–45.
[48] Dwarshuis NJ, et al. Functionalized microcarriers improve T cell manufacturing by facilitating migratory memory T cell production and increasing CD4/CD8 ratio. Cold Spring Harbor Laboratory; 2019.
[49] Odeh-Couvertier VY, et al. Predicting T-cell quality during manufacturing through an artificial intelligence-based integrative multiomics analytical platform. Bioengineering & Translational Medicine 2022.
[50] Sahoo P, et al. Mathematical deconvolution of CAR T-cell proliferation and exhaustion from real-time killing assay data. J. R. Soc. Interface 2020;17(162):20190734.
[51] Xi B, et al. A real-time potency assay for chimeric antigen receptor T cells targeting solid and hematological cancer cells. J. Vis. Exp. 2019(153).
[52] Long AH, et al. 4-1BB costimulation ameliorates T cell exhaustion induced by tonic signaling of chimeric antigen receptors. Nat. Med. 2015;21(6):581–90.
[53] Davenport AJ, et al. CAR-T cells inflict sequential killing of multiple tumor target cells. Cancer Immunol. Res. 2015;3(5):483–94.
[54] Ramello MC, et al. An immunoproteomic approach to characterize the CAR interactome and signalosome. Sci. Signal 2019(568):12.
[55] Salter AI, et al. Phosphoproteomic analysis of chimeric antigen receptor signaling reveals kinetic and quantitative differences that affect cell function. Sci. Signal 2018;11(544).
[56] Brentjens RJ, et al. Safety and persistence of adoptively transferred autologous CD19-targeted T cells in patients with relapsed or chemotherapy refractory B-cell leukemias. Blood 2011;118(18):4817–28.
[57] Davila ML, et al. Efficacy and toxicity management of 19-28z CAR T cell therapy in B cell acute lymphoblastic leukemia. Sci. Transl. Med. 2014;6(224):224ra25.
[58] Grupp SA, et al. Chimeric antigen receptor-modified T cells for acute lymphoid leukemia. N. Engl. J. Med. 2013;368(16):1509–18.
[59] Jensen MC, et al. Antitransgene rejection responses contribute to attenuated persistence of adoptively transferred CD20/CD19-specific chimeric antigen receptor redirected T cells in humans. Biol. Blood Marrow Transplant. 2010;16(9):1245–56.
[60] Kalos M, et al. T cells with chimeric antigen receptors have potent antitumor effects and can establish memory in patients with advanced leukemia. Sci. Transl. Med. 2011;3(95):95ra73.
[61] Kochenderfer JN, et al. B-cell depletion and remissions of malignancy along with cytokine-associated toxicity in a clinical trial of anti-CD19 chimeric-antigen-receptor-transduced T cells. Blood 2012;119(12):2709–20.
[62] Porter DL, et al. Chimeric antigen receptor-modified T cells in chronic lymphoid leukemia. N. Engl. J. Med. 2011;365(8):725–33.
[63] Lin-Gibson S, Rogers KC, Plant AL. Measurement challenges for CAR-T biomanufacturing: highlights from a meeting sponsored by the National Institute of Standards and Technology (NIST). Hum Gene Ther Clin Dev 2016;27(2):66–8.
[64] Bravery CA, et al. Potency assay development for cellular therapy products: an ISCT review of the requirements and experiences in the industry. Cytotherapy 2013;15(1):9–19.
[65] Freeman AJ, et al. Unleashing TNF cytotoxicity to enhance cancer immunotherapy. Trends Immunol. 2021;42(12):1128–42.
[66] Kearney CJ, et al. Tumor immune evasion arises through loss of TNF sensitivity. Sci Immunol 2018;3(23).
[67] Malissen B, Bongrand P. Early T cell activation: integrating biochemical, structural, and biophysical cues. Annu. Rev. Immunol. 2015;33:539–61.
[68] Leone RD, et al. Glutamine blockade induces divergent metabolic programs to overcome tumor immune evasion. Science 2019;366(6468):1013–21.
[69] Lian G, et al. Glutathione de novo synthesis but not recycling process coordinates with glutamine catabolism to control redox homeostasis and directs murine T cell differentiation. Elife 2018: 7.
[70] Chapman NM, Boothby MR, Chi H. Metabolic coordination of T cell quiescence and activation. Nat. Rev. Immunol. 2020;20(1):55–70.
[71] Bensinger SJ, et al. LXR signaling couples sterol metabolism to proliferation in the acquired immune response. Cell 2008;134(1):97–111.
[72] Xu X, et al. A metabolism toolbox for CAR T therapy. Front. Oncol. 2019;9:322.
[73] Ardawi MS. Glutamine and glucose metabolism in human peripheral lymphocytes. Metabolism 1988;37(1):99–103.
[74] Carr EL, et al. Glutamine uptake and metabolism are coordinately regulated by ERK/MAPK during T lymphocyte activation. J. Immunol. 2010;185(2):1037–44.
[75] Sommermeyer D, et al. Chimeric antigen receptor-modified T cells derived from defined CD8+ and CD4+ subsets confer superior antitumor reactivity in vivo. Leukemia 2016;30(2):492–500.
[76] Kawalekar OU, et al. Distinct signaling of coreceptors regulates specific metabolism pathways and impacts memory development in CAR T cells. Immunity 2016;44(3):712.
[77] Zhao X, et al. Efficacy and safety of CD28- or 4-1BB-Based CD19 CAR-T cells in B cell acute lymphoblastic leukemia. Mol Ther Oncolytics 2020;18:272–81.
[78] Guidance Document: Potency Tests for Cellular and Gene Therapy Products. FDA; 2015 Editor.